A Journal of the Gesellschaft Deutscher Chemiker

Angewandte International Edition GDCh Chemie

www.angewandte.org

Accepted Article

Title: Negative pressure pyrolysis induced highly accessible single sites dispersed on 3D graphene frameworks for enhanced oxygen reduction

Authors: Yuen Wu, Huang Zhou, Tong Yang, Zongkui Kou, Lei Shen, Yafei Zhao, Zhiyuan Wang, Xiaoqian Wang, Jie Xu, Min Chen, Lin Tian, Wenxin Guo, Qiuping Wang, Hongwei Lv, Wenxing Chen, Xun Hong, Jun Luo, and Daping He

To be cited as: *Angew. Chem. Int. Ed.* 10.1002/anie.202009700

Link to VoR: https://doi.org/10.1002/anie.202009700

WILEY-VCH

10.1002/anie.202009700

WILEY-VCH

COMMUNICATION

Negative pressure pyrolysis induced highly accessible single sites dispersed on 3D graphene frameworks for enhanced oxygen reduction

Dr.Huang Zhou,[a,b,c]† Dr.Tong Yang,[d]† Dr.Zongkui Kou,[d] Dr.Lei Shen,[e] Dr.Yafei Zhao,[a] Dr. Zhiyuan Wang, Dr.Xiaoqian Wang,[a] Dr. Zhenkun Yang,[a] Dr. Junyi Du, [a] Dr.Jie Xu,[f] Min Chen,[a] Lin Tian,[a] Wenxin Guo,[a] Qiuping Wang,[a] Hongwei Lv,[a] Dr.Wenxing Chen,[g] Prof.Xun Hong,[a] Prof.Jun Luo,[f] Prof.Daping He, [b]* Prof.Yuen Wu[a,c]*

Abstract: The surface structure of supports is related to the properties of catalytic sites and their spatial structure also plays a dominant role in the mass transfer during catalysis process. Herein, we report a negative pressure pyrolysis to access dense single metal sites (Co, Fe, Ni etc.) with high accessibility dispersed on three-dimensional (3D) graphene frameworks (GFs), during which the differential pressure between inside and outside of metal-organic frameworks (MOFs) promotes the cleavage of the derived-carbon layers and gradual expansion of mesopores. In situ transmission electron microscopy and Brunauer-Emmett-Teller tests reveal the formed 3D GFs possess an enhanced mesoporosity and external surface area, which greatly favor the mass transport and utilization of metal sites. This contributes to an excellent oxygen reduction reaction (ORR) activity (with a half-wave potential of 0.901 V vs. RHE). Theoretical calculations verify that selective carbon cleavage near Co centers can efficiently lower the overall ORR theoretical overpotential in comparison with intact atomic configuration. This work discovers the structure-property correlations that provides an idea of designing highly accessible catalysts for practical applications.

Single site catalysts are usually composed of the central metal sites and the defective supports such as oxides, carbon materials and zeolites.[1] The local electric structure of central metal sites usually determines the intrinsic activity.[1b, 2] Towards more practical industrial applications, the mass transfer and the corresponding mass activity are highly dependent on the spatial three-dimensional (3D) structure of the support.[3] Metal-organic frameworks (MOFs) derived metal-nitrogen sites confined within carbon (M-N_x/C) have emerged as remarkable single site catalysts in various important reactions such as hydrogen and oxygen evolution, oxygen and CO_2 reduction due to their high metal loading and uniform coordination.[1b, 4] As most of M-N_x sites are hosted within the micropores on the MOFs-derived carbon substrate,[5] only a few proportion of the obtained M-N_x sites can be utilized as active sites. That means facilitating the contact between the M-N_x sites and the reactants with high accessibility is crucial for the design of single site catalysts. Especially for oxygen reduction reaction (ORR) catalysts used in the cathode of proton exchange membrane fuel cells (PEMFCs), the excessively inactive components can vastly slow down the mass transports and increase the internal ohmic resistance, thereby degrading the overall efficiency and durability of the fuel cell.[3, 6]

Herein, we report a negative pressure pyrolysis strategy that can directly transform 3D MOFs into 3D graphene frameworks (GFs) at high temperatures, which enables the supported single-atom metal sites (Co/Fe/Ni SAs) with excellent accessibility and stability. Compared with the MOFs-derived carbon substrates prepared by conventional pyrolysis,[9,5b] the obtained 3D GFs exhibit an enhanced mesoporosity and external surface area. More importantly, by adjusting the differential gas pressure inside and outside of the heating equipment/quartz tube, we can realize the precise regulation of mesoporosity of the carbon substrate and accessibility of the supported single metal sites. In particular, the resultant Co SAs/3D GFs catalyst exhibits a superior ORR activity to most of the reported Co-based nanoparticles and single Co sites catalysts. Mechanism exploration by in-situ transmission electron microscopy (TEM) and density functional theory (DFT) calculations suggest that a negative pressure can facilitate the selective cleavage of carbon layers and evaporation of unstable atoms at designed temperatures, which can induce defects adjacent to metal centers, thus lowering the overall ORR overpotential.

The specific preparation route of Co SAs/3D GFs is displayed in Fig.1a. Employing both zinc and cobalt ion as metallic nodes, 2-methylimidazole as organic linkers, and methanol as solvent, a type of bimetallic ZnCo-MOFs rhombododecahedron (Fig. S1) was firstly synthesized by a solvent method.[4b] The obtained ZnCo-MOFs were subsequently transferred into a ceramic boat and sealed in a corundum quartz tube, in which the differential pressure (inside vs. outside) was remained at ΔP=-0.02 MPa after repeatedly washing by nitrogen. It is noted that the gas pressure inside the MOFs remained intact even after the tube was under negative pressure due to the microporous nature of MOFs. Then the sample was rapidly heated to 900°C and kept at that temperature for 3 h. During the annealing, the pyrolysis process would accelerate the generation of gas inside the MOFs, which

[a] H. Zhou, Y. Zhao, Z. Wang, X. Wang, Z. Yang, J. Du, M. Chen, L. Tian, W. Guo, Q. Wang, H. Lv, X. Hong, Y. Wu
Department of Chemistry, iChEM (Collaborative Innovation Center of Chemistry for Energy Materials), University of Science and Technology of China, Hefei 230026, China
E-mail: yuenwu@ustc.edu.cn
[b] H. Zhou, D. He
Hubei Engineering Research Center of RF-Microwave Technology and Application, School of Science, Wuhan University of Technology, Wuhan 430070, China
E-mail: hedaping@whut.edu.cn
[c] H. Zhou Y. Wu
Dalian National Laboratory for Clean Energy, Dalian 116023, China
[d] T. Yang, Z. Kou
Department of Physics, National University of Singapore, Singapore 117551, Singapore
[e] L. Shen
Department of Mechanical Engineering, National University of Singapore, Singapore 117575, Singapore
[f] J. Xu, J. Luo
Laboratory of Advanced Functional Porous Materials, Institute for New Energy Materials & Low-Carbon Technologies, School of Materials Science and Engineering Tianjin University of Technology Tianjin 300384, China
[g] W. Chen
Beijing Key Laboratory of Construction Tailorable Advanced Functional Materials and Green Applications, School of Materials Science and Engineering, Beijing Institute of Technology, Beijing 100081, China
† These authors contributed equally.

10.1002/anie.202009700

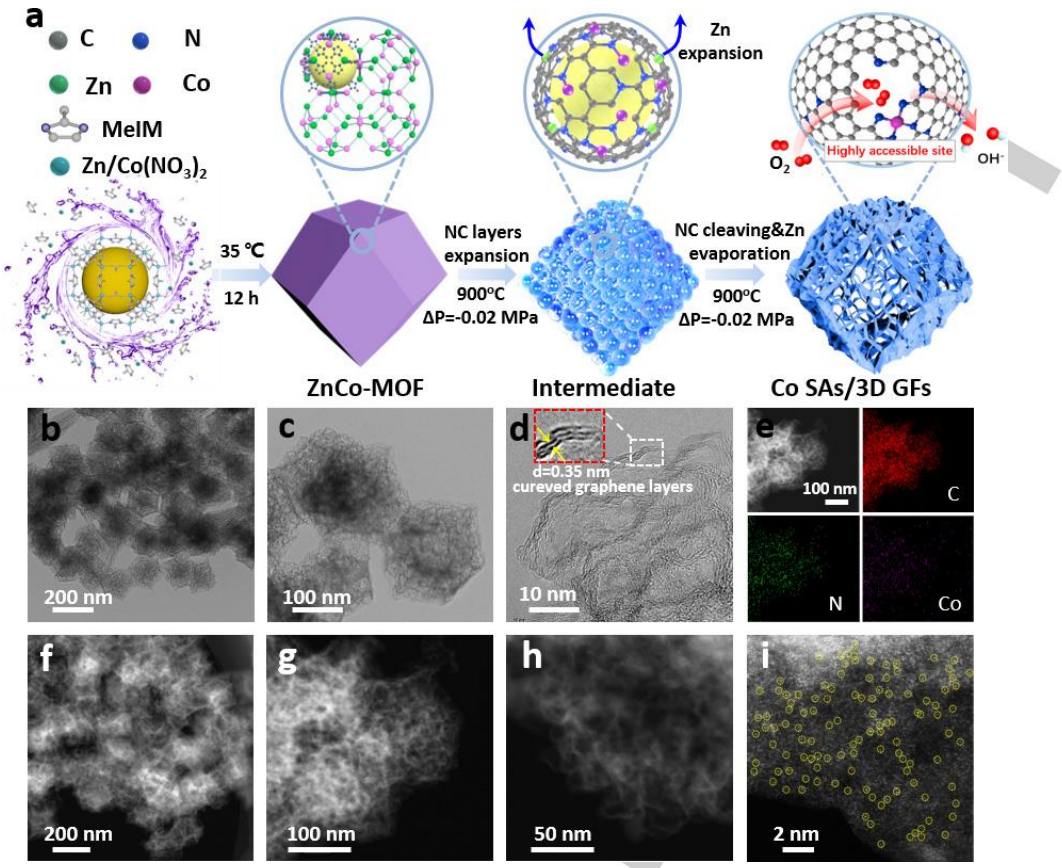

Figure 1. (a) Schematic illustration, (b-d) TEM, (e) EDS mappings, and (f-i) HAADF-STEM images of Co SAs/3D GFs.

would expand the cavity of MOFs. The differential pressure inside and outside of the MOFs promoted the gradual expansion and cleavage of the derived-carbon layers, resulting in the formation of 3D graphene frameworks (Fig.1a).This process is just like a "balloon effect", in which the difference between the internal and external gas pressure determines the inflation and rupture of balloon. Meanwhile, the Zn nodes reduced by carbonization of the organic linker were evaporated due to the low boiling point (bp 907°C). In contrast, the Co nodes remained atomic dispersion on 3D GFs (Co SAs/3D GFs) due to the high boiling point. TEM (Fig.1b-d and S2) and high-angle annular dark-field scanning transmission electron microscopy (HAADF-STEM, Fig.1f-h) images exhibit that Co SAs/3D GFs possess a hollow framework structure, which is totally different from Co SAs supported on nitrogen-doped and microporous carbon substrates prepared by conventional strategy (Co SAs/NC, Fig.S3 and S4).[4b, 7] N_2 adsorption-desorption isotherms reveal that the mesoporosity increases significantly, as demonstrated by the hysteresis loop in N_2 adsorption-desorption isotherms of Co SAs/3D GFs, and the specific surface area increases from 591.66 to 915.47 m^2/g (Fig.S5). The pore sizes distribution further confirms that the mesopores for Co SAs/3D GFs are mainly centered at 4.0 nm (Fig. S6). Also, Fig.1b-d reveal that no Co nanoparticles were found on the 3D GFs and energy dispersive X-ray spectroscopy (EDS) mappings in Fig. 1e suggest that the Co species are uniformly dispersed, indicating the atomic dispersion of these Co species. High-resolution TEM (HRTEM) images (Fig.1d and Fig.S2) further reveal the presence of 3-layer curved graphene with a layer distance of 0.35 nm, whereas the dominating carbon for Co SAs/NC is amorphous (Fig.S3). This could also be verified by the enhanced 2D peak of Co SAs/3D GFs in Raman spectra versus Co SAs/NC (Fig. S7). Aberration-corrected (AC) HAADF-STEM was further used to determine the exact morphology on the surface of 3D GFs. As shown in Fig.1i, the dense atomically dispersed bright dots (circled in yellow) could be assigned to the heavier Co atoms in comparison with N and C, demonstrating that the Co species on the surface of 3D GFs are indeed atomically dispersed.

XRD patterns (Fig.2a) exhibit that the synthesized ZnCo-MOFs possess similar peaks with that of zeolite imidazolate frameworks-8 (ZIF-8), indicating the Zn nodes replaced by Co adopt the similar crystal structure. After being heated at 900°C for 3h, the typical signal of MOFs vanished and only two wide peaks at 2θ=20~30° and 40~45° corresponded to carbon (002) and (100)/(101) peaks emerged. Also, there is no crystalline Co signal observed in XRD pattern for Co SAs/3D GFs. These results suggest that the ZnCo-MOFs were completely transformed into carbon with the absence of Co nanoparticles and clusters. XPS measurement was used to trace the element changes over the whole annealing process (Fig.S8). Table S1 reveals that the Zn element on surface decreases from 8.3 % at initially to 0.17 % eventually, accompaning with the dramatical decrease of N element (26.25 vs 7.56 %), indicating the simultaneous evaporation of Zn and N during the annealing (Fig.S9 and Fig. 2b). The N type (Fig. 2b) is

10.1002/anie.202009700

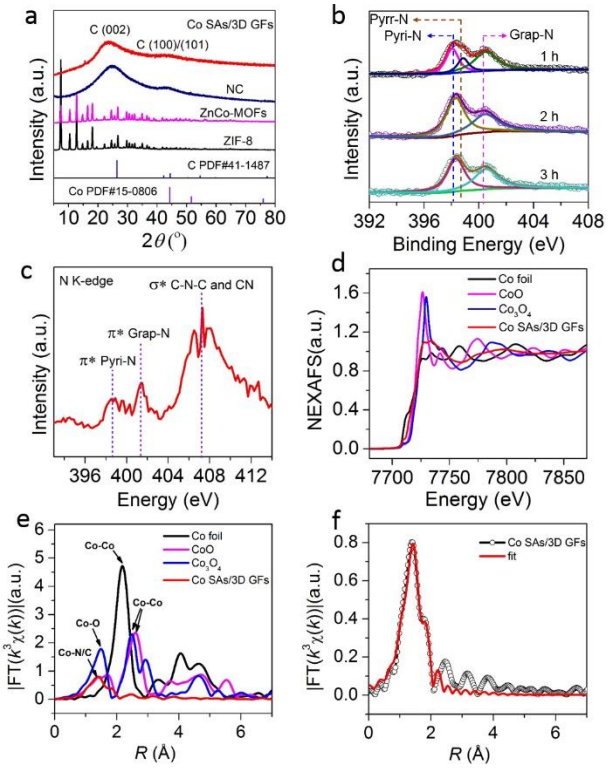

Figure 2. (a) XRD patterns of Co SAs/3D GFs and references, (b) N 1s XPS spectra of ZnCo-MOFs annealing with different time at 900ºC. (c) N K-edge and (d) Co K-edge NEXAFS spectra, and (e) EXAFS spectra and (f) the corresponding fitting curve for Co K-edge of Co SAs/3D GFs.

transferred from pyrr-N to pyri-N (398.1 eV) and graph-N (400.6 eV).[8] This result can be also demonstrated by characterization of the near edge X-ray absorption fine structure (NEXAFS). Fig.2c reveals the existence of three main peaks (398.5 eV, 401.6 eV and 407.4 eV)[9] in the spectrum of Co SAs/3D GFs, corresponding to the π* excitation of pyri-N and graph-N and σ* excitation of C−N, respectively. Because one p-electron for pyri-N is donated to π conjugated system,[10] the pyri-N can stabilize the Co SAs efficiently. As expected, the Co element (1.16±0.03 %) collected by XPS keeps almost the same with the annealing time (Table S1), in good consistent with the unchanged ICP results (1.38±0.05 wt%, Table S2).

High-resolution XPS spectra of Co 2p (Fig. S10) show that the binding energy of Co $2p_{3/2}$ peak for Co SAs (780.0 eV) is positive than that of Co^0 (778.1 eV) and negative than that of Co^{3+} (781.1 eV),[11] illustrating the chemical valence of Co SAs is between Co(0) and Co(Ⅲ). The ionic nature of Co SAs could also be verified by NEXAFS spectrum of Co K-edge (Fig.2d), in which the absorption threshold position for Co SAs is located between Co foil and Co_3O_4. Additionally, extended-XAFS (EXAFS) experiment (Fig.2e) and data fitting (Fig.2f) were performed to determine the coordination environment of the obtained Co SAs. There is only one remarkable peak (1.48 Å) in the region 1 to 2 Å from the Co-N coordination and no peaks in the region 2 to 3 Å from the Co-Co coordination, demonstrating the sole presence of single atoms in Co SAs/3D GFs. The fitting result confirms that the Co-N

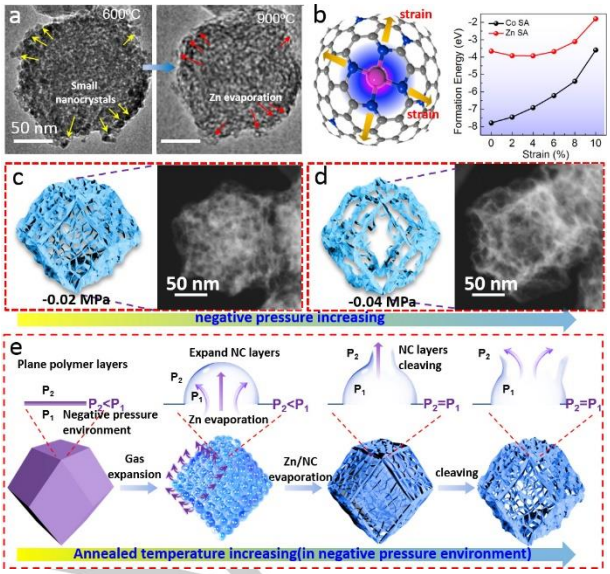

Figure 3. (a) In-situ TEM images for the formation of Co SAs/3D GFs. (b) Schematic illustration of MN_4 (M=Co, Zn) with strain and the calculated dependence of the formation energy of the M SA on the biaxial strain in MN_4. (c,d) Schematic illustration and the corresponding HAADF images of Co SAs/3D GFs obtained at different pressure. (e) Mechanism illustration of the formation of Co SAs/3D GFs.

coordination number is 4, revealing that a single Co atom is coordinated with 4 N atoms. More fitting curves and parameters can be seen in Fig. S12 and S13 and Table S3.

In-situ TEM measurement was used to acquire images at different stage of the evolution from ZnCo-MOFs to Co SAs/3D GFs. Representative images in Fig.3a reveal that ZnCo-MOFs at low temperature (600ºC) tended to decompose into small nanocrystals, due to the generation of volatile gas inside the MOFs. This can be also revealed by static TEM images, during which the cavity of MOFs was greatly expanded (Fig.S14). When the annealing temperature was elevated to 900ºC, the Zn nodes of MOFs would become unstable and be rapidly evaporated. Meanwhile, the ligands converted into stable graphited carbon layers, which were largely retained at high temperatures, contributing to the robust 3D GFs. DFT calculations were also performed to gain an insight into the evolution of ZnCo-MOFs in a negative pressure environment. Note that a negative pressure gives rise to a remarkable tensile strain on ZnCo-MOFs. Therefore, we investigated the stability of the single metal atom (M SA, M=Zn, Co) in the defect-free MN_4 and their dependence on the tensile strain (Fig.3b). The formation energy is defined as $E_{form}(M)=E(MN_4)-E(V_M)-E(M)$, where $E(MN_4)$ and $E(V_M)$ are the total energy of the MN_4 with and without the M SA, respectively. $E(M)$ is the energy of a single M atom. As shown in Fig.3b and Table S4, the Co SA is much more energetically stable than the Zn SA in the absence of the biaxial tensile strain. As the MN_4 is stretched, E_{form} increases for both Co and Zn SA, among which the Co SA remains more stable. The higher slope associated with the Co SA suggests stronger Co-N bonding than the counterpart for the Zn SA. Our calculations also show that the further increase

in the tensile strain (>10%) will lead to cracking of MN_4. On the whole, the Zn SAs in the ZnCo-MOF might be easier to evaporate than the Co SAs at high temperatures in a negative pressure environment. These results indicate that the negative pressure environment may facilitate the evaporation of unstable atoms, resulting in the rapid Zn evaporation and cleavage of NC layers, whereas the highly stable atoms with strong coordination are retained. To further determine the effect of negative pressure environment, the ΔP=-0.02 MPa was increased to -0.04 MPa (Fig.3c and d and S15). Strikingly, more N/C atoms were evaporated and the 3D GFs structure with larger pores were formed. Similarly, Fe SAs/3D GFs (Fig. S16) and Ni SAs/3D GFs (Fig. S17) can be also prepared under the comparable condition, revealing the good generality of this strategy. Based on above results, a more detail intrinsic mechanism of the formation of M SAs/3D GFs (M=Co, Fe, Ni etc.) is shown in Fig. 3e. Firstly, the MOFs at low temperatures tend to expand and form many fragmented nanocrystals due to the rapid gas expansion induced by differential pressure inside and outside of the MOFs. Meanwhile, the expanded NC layers begin to crack, accompanied with the evaporation of rocking N and C atoms, resulting in the formation of 3D GFs.

Oxygen reduction reaction (ORR) catalyst is an important constituent part in cathode of PEMFCs and Zn-air batteries, which determines the eventual power density and energy conversion efficiency.[4c, 12] To understand the structure-property relationships of the prepared Co SAs catalysts, the ORR test was performed. We found that the obtained Co SAs/3D GFs can reach a high onset potential (E_0=1.032 V) and half-wave potential ($E_{1/2}$=0.901 V) in a 0.1 M KOH solution (Fig.4a), suppressing those of Pt/C (E_0= 1.004 V, $E_{1/2}$= 0.835 V), Co SAs/NC (E_0= 0.992 V, $E_{1/2}$= 0.840 V), the NC derived from ZIF-8 (Fig. S18 and S19, E_0 = 0.768 V, $E_{1/2}$= 0.691 V) and most of the reported Co-based materials (Table S5). Also, the kinetic current density (J_k) at 0.85 V for the prepared catalysts and Pt/C were further compared (Fig.4b), in which the Co SAs/3D GFs exhibit the most outstanding performance. This result was further confirmed by the smallest Tafel slope (Fig.S21) of Co SAs/3D GFs(Co SAs/3D GFs(~71 mV dec^{-1})<Co SAs/NC(~73 mV dec^{-1})<Pt/C(~82 mV dec^{-1})<NC(~105 mV dec^{-1})). The electrochemical double-layer capacitance (C_{dl}) value of Co SAs/3D GFs (17.3 mF cm^{-2}) is considerably higher than that of Co SAs/NC (13.8 mF cm^{-2}), indicating the enhanced exposure of active sites for ORR in the former (Fig.S22). The high electron transfer rate of Co SAs/3D GFs was verified by the rotating ring disk electrode (RRDE) tests and the Koutecky–Levich (K-L) plots (the calculated transfer number is 3.99), demonstrating a near four-electron ORR pathway over Co single sites (Fig.S23). Furthermore, the durability experiment (Fig.4c) reveals no obvious decay in $E_{1/2}$ after 5,000 continuous potential cycles, suggesting the superior catalytic stability. Similarly, Co SAs/3D GFs (Fig.S24) exhibit no observable current density decay after 100 s upon injecting methanol (1 M). Careful examination of HAADF, AC HAADF-STEM and EDS measurements exhibit no observable changes of morphology, further demonstrating the excellent structure stability of Co SAs/3D GFs after recycling (Fig.S26 and S27). Furthermore, as the cathode catalyst in Zn-air battery, Co SAs/3D GFs based catalyst can reach a maximum power density of 206 mV cm^{-2} at 0.67 V, which is 26 mV cm^{-2} higher than that of commercial Pt/C at same potential and higher than most of reported catalysts (Table S6). A long-term charge-discharge cycling tests further reveal that Co SAs/3D GFs possess a better stability than Pt/C (Fig.4d). Also, three assembled all-solid-state batteries by using Co SAs/3D GFs+RuO_2 as the cathode catalyst can light a small bulb (Fig.S28 and S29).

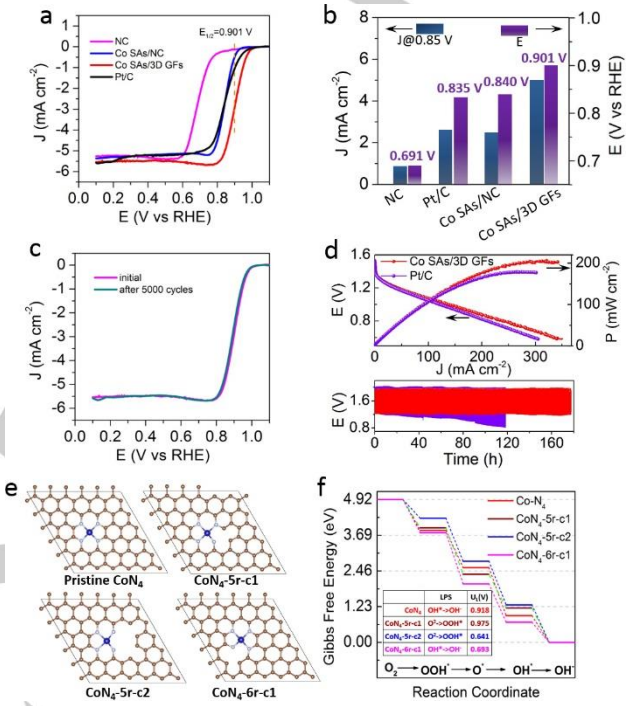

Figure 4. (a) LSV curves. (b) Comparison of J and $E_{1/2}$ for different catalysts. (c) Stability test. (d) Discharge curves of Zn–air batteries and Galvanostatic discharge-charge cycling profiles at 5 mA cm^{-2} (inset) of Co SAs/3D GFs+RuO_2 and Pt/C+RuO_2 electrodes. (e) Four possible atomic configurations (r5 or r6 refers to the five- or six-membered Co-N heterocyclic ring, respectively; 1 or 2 refers to one or two C-N bond adjacent to CoN_4, respectively). (f) Free energy diagram of different configurations along the 4*e*⁻ ORR pathway.

DFT calculations were further conducted to understand the enhanced ORR activity. Based on the HAADF, XAFS and XPS characterization results for the Co SAs/3D GFs, we constructed three possible models of defective CoN_4 structure, *i.e.* CoN_4-5r-c1, CoN_4-5r-c2 and CoN_4-6r-c1 (Fig. 4e). For comparison, the pristine Co-N_4 was also constructed. The formation energies (Fig.S30) demonstrate that the defective CoN_4-5r-c1 (5.864 eV) is lower than those of CoN_4-6r-c1 (6.321 eV) and defective graphene (7.720 eV). Also, we calculated the Gibbs free energy change on the defect-free and defective CoN_4 along the 4*e*⁻ ORR process, as shown in Fig. 4f and Table S7. For the defect-free CoN_4, the limiting potential step (LPS) of ORR is the reduction of OH^* with $U_L(CoN_4)$=0.918 V, namely $\eta_{theo}(CoN_4)$=0.312 V. In the presence of an adjacent carbon vacancy, LPS on CoN_4-6r-c1 remains unchanged, but the OH^* adsorption is much stronger than that on the pristine CoN_4, leading to an inferior ORR activity

($U_L(CoN_4\text{-}6r\text{-}c1)$=0.693 V;$\eta_{theo}(CoN_4\text{-}6r\text{-}c1)$=0.537 V). Similarly, an inferior activity is found for CoN_4-5r-c2, on which LPS changes to the reduction of O_2 due to the weak stabilization of OOH^*, *i.e.* $U_L(CoN_4\text{-}5r\text{-}c2)$=0.641 V and $\eta_{theo}(CoN_4\text{-}5r\text{-}c2)$=0.589 V. On the contrary, the calculations show that ORR on CoN_4-5r-c1 has a lower theoretical overpotential $\eta_{theo}(CoN_4\text{-}5r\text{-}c1)$=0.225 V than on the pristine CoN_4, indicating an improved ORR activity. The above analysis manifests that the adjacent defects (vacancies) have a significant impact on the ORR activity of the Co SAs. Moreover, the selective cleavage of carbon layers to generate CoN_4-5r-c1 center is likely responsible for the enhanced ORR activity of the Co SAs/3D GFs observed in our experiments.

In summary, we have developed a negative pressure pyrolysis strategy that allows us to controllably prepare a series of single metal sites supported on three-dimensional graphene frameworks with high accessibility and stability, which greatly increases the utilization and catalytic efficiency of the supported metal atoms. Our findings not only open up a new way of preparing highly accessible single site catalysts, but also provide an understanding of defect engineering of single metal sites to enhance their catalytic performance.

Acknowledgements

This work was supported by National Key R&D Program of China 2017YFA (0208300) and (0700104), the National Natural Science Foundation of China (21522107, 21671180), the DNL Cooperation Fund, CAS (NDL201918) and the Fujian Institute of Innovation, CAS. We thank the photoemission endstations BL1W1B in Beijing Synchrotron Radiation Facility (BSRF), BL14W1 in Shanghai Synchrotron Radiation Facility (SSRF), BL10B and BL11U in National Synchrotron Radiation Laboratory (NSRL) for the help in characterizations.We thank the Centre for Advanced 2D Materials, National University of Singapore, for providing the high performance supercomputing resources.

Keywords: negative pressure • single sites • 3D graphene frameworks • metal-organic frameworks • oxygen reduction reaction

[1] a) L. Nie, D. Mei, H. Xiong, B. Peng, Z. Ren, X. Hernandez, A. DeLaRiva, M. Wang, M. Engelhard, L. Kovarik, A. Datye, Y. Wang, *Science* **2017**, *358*, 1419-1423; b) Z. Li, S. Ji, Y. Liu, X. Cao, S. Tian, Y. Chen, Z. Niu, Y. Li, *Chem. Rev.* **2020**, *120*, 623-682; c) B. Qiao, A. Wang, X. Yang, L. F. Allard, Z. Jiang, Y. Cui, J. Liu, J. Li, T. Zhang, *Nat. Chem.* **2011,***3*, 634-641; d) Y. Jia, K. Jiang, H. Wang, X. Yao, *Chem* **2019**, *5*, 1371-1397; e) Z. Zhang, J. Sun, F. Wang, L. Dai, *Angew. Chem. Int. Ed.* **2018**, *57*, 9038-9043.

[2] a) J. Zhang, Y. Zhao, C. Chen, Y.-C. Huang, C.-L. Dong, C.-J. Chen, R.-S. Liu, C. Wang, K. Yan, Y. Li, G. Wang, *J. Am. Chem. Soc.* **2019**, *141*, 20118-20126; b) R. Ding, Y. Liu, Z. Rui, J. Li, J. Liu, Z. Zou, *Nano Res.* **2020**, *13*, 1519-1526.

[3] M. Shao, Q. Chang, J.-P. Dodelet, R. Chenitz, *Chem. Rev.* **2016**, *116*, 3594-3657.

[4] a) Y. Qu, Z. Li, W. Chen, Y. Lin, T. Yuan, Z. Yang, C. Zhao, J. Wang, C. Zhao, X. Wang, F. Zhou, Z. Zhuang, Y. Wu, Y. Li, *Nat. Cat.* **2018**, *1*, 781-786; b) P. Yin, T. Yao, Y. Wu, L. Zheng, Y. Lin, W. Liu, H. Ju, J. Zhu, X. Hong, Z. Deng, G. Zhou, S. Wei, Y. Li, *Angew. Chem. Int. Ed.* **2016**, *55*, 10800-10805; c) Z. Song, N. Cheng, A. Lushington, X. Sun, *Catalysts* **2016**, *6*, 116; d) B. K. Kang, S. Y. Im, J. Lee, S. H. Kwag, S. B. Kwon, S. Tiruneh, M.-J. Kim, J. H. Kim, W. S. Yang, B. Lim, D. H. Yoon, *Nano Res.* **2019**, 12, 1605-1611.

[5] a) X. Wan, X. Liu, Y. Li, R. Yu, L. Zheng, W. Yan, H. Wang, M. Xu, J. Shui, *Nat. Catal.* **2019**, *2*, 259-268; b) H. Zhang, S. Hwang, M. Wang, Z. Feng, S. Karakalos, L. Luo, Z. Qiao, X. Xie, C. Wang, D. Su, Y. Shao, G. Wu, *J. Am. Chem. Soc.* **2017**, *139*, 14143-14149.

[6] H. T. Chung, D. A. Cullen, D. Higgins, B. T. Sneed, E. F. Holby, K. L. More, P. Zelenay, *Science* **2017**, *357*, 479-484.

[7] X. X. Wang, D. A. Cullen, Y.-T. Pan, S. Hwang, M. Wang, Z. Feng, J. Wang, M. H. Engelhard, H. Zhang, Y. He, Y. Shao, D. Su, K. L. More, J. S. Spendelow, G. Wu, *Adv. Mater.* **2018**, *30*, 1706758.

[8] D. Li, Y. Jia, G. Chang, J. Chen, H. Liu, J. Wang, Y. Hu, Y. Xia, D. Yang, X. Yao, *Chem* **2018**, *4*, 2345-2356.

[9] Z. Yasong, W. Jiawei, Y. Huiying, Z. Lijuan, L. Kaifeng, W. Lei, Y. Nailiang, L. Daobin, S. Li, Z. Jia, *Nat. Chem.* **2018**,10, 924-931.

[10] J. Casanovas, J. M. Ricart, J. Rubio, F. Illas, J. M. Jimenez-Mateos, *J. Am. Chem. Soc.* **1996**, *118*, 8071-8076.

[11] Y. Pan, R. Lin, Y. Chen, S. Liu, W. Zhu, X. Cao, W. Chen, K. Wu, W.-C. Cheong, Y. Wang, L. Zheng, J. Luo, Y. Lin, Y. Liu, C. Liu, J. Li, Q. Lu, X. Chen, D. Wang, Q. Peng, C. Chen, Y. Li, *J. Am. Chem. Soc.* **2018**, *140*, 4218-4221.

[12] a) J. Fu, Z. P. Cano, M. G. Park, A. Yu, M. Fowler, Z. Chen, *Adv. Mater.* **2017**, *29*, 1604685; b) H. Jin, H. Zhou, P. Ji, C. Zhang, J. Luo, W. Zeng, C. Hu, D. He, S. Mu, *Nano Res.* **2020**, *13*, 818-823.

10.1002/anie.202009700

WILEY-VCH

COMMUNICATION

Entry for the Table of Contents

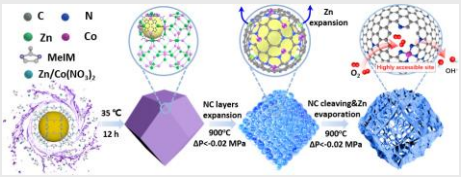

We report a negative pressure pyrolysis to access dense single metal sites (Co, Fe, Ni etc.) with high accessibility dispersed on three-dimensional graphene frameworks, during which the differential pressure between inside and outside of metal-organic frameworks promotes the cleavage of the derived-carbon layers and gradual expansion of mesopores. The formed 3D GFs possess an enhanced mesoporosity and external surface area, which greatly favor the mass transport and utilization of metal sites. This contributes to an excellent oxygen reduction reaction (ORR) activity because the selective carbon cleavage near Co centers can efficiently lower the overall ORR theoretical overpotential.

*Author(s), Corresponding Author(s)**

Huang Zhou,† Tong Yang,† Zongkui Kou, Lei Shen, Yafei Zhao, Zhiyuan Wang, Xiaoqian Wang, Jie Xu, Min Chen, Lin Tian, Wenxin Guo, Qiuping Wang, Hongwei Lv, Wenxing Chen, Xun Hong, Jun Luo, Daping He, Yuen Wu**

Page No. – Page No.

Negative pressure pyrolysis induced highly accessible single sites dispersed on 3D graphene frameworks for enhanced oxygen reduction